JOURNAL OF Applied Polymer SCIENCE

Effect of Magnetic Field on Discotic Nematic Liquid Crystalline Polymers under Simple Shear Flow

Shu-Fang Fu, Jing-Bai, Xuan-Zhang Wang

Key Laboratory for Photonic and Electric Bandgap Materials, Ministry of Education, Heilongjiang Key Laboratory for Low Dimensional System Mesoscopic Physics, School of Physics and Electronic Engineering, Harbin Normal University, Harbin 150025, People's Republic of China

Correspondence to: S.-F. Fu (E-mail: shufangfu@yahoo.com)

ABSTRACT: The effect of magnetic field on the discotic nematic liquid crystalline polymers (LCPs) is analyzed with the extended Doi theory, in which the molecular shape parameter (β) is defined at -1.0. The evolution equation for the probability function of the discotic nematic LCP molecules is solved without any closure approximations. The transition among flow-orientation modes, such as tumbling, wagging, and aligning defined similar to the rodlike LCPs, is strongly affected by the magnetic fields. The new aligning flow-orientation mode observed for the rodlike LCPs under magnetic fields also can be investigated in the lower shear rate region. On the other hand, the effect of magnetic fields parallel to the x- and y-axis on the time-averaged first and second normal stress differences ($\bar{N}_1^*$, $\bar{N}_2^*$) are also studied. It can be seen that the shear rate regions of the sign changes of $\bar{N}_1^*$, $\bar{N}_2^*$ are completely contrary to those conclusions achieved for the rodlike LCPs. In addition, the absolute values of $\bar{\eta}^*$ increase with the magnetic field strength in the lower shear rate range owing to the new aligning flow-orientation mode. Finally, the flow-phase diagram versus β is also discussed. © 2012 Wiley Periodicals, Inc. J. Appl. Polym. Sci. 000: 000–000, 2012

KEYWORDS: polymer rheology; simulations; rheology

Received 4 February 2012; accepted 26 June 2012; published online
DOI: 10.1002/app.38268

INTRODUCTION

Nematic phase in liquid crystals (LCs) is the simplest mesophase in which an orientational order exists, but there is no positional order. This simple mesophase can be formed by two drastically different configurations: rodlike and discotic LCs. The nematic phase of discotic LCs is quite similar to the one of rodlike LCs. However, the optical feature of these two kinds of LCs is different: the common rodlike LCs exhibit uniaxial positive birefringence, whereas the discotic LCs intrinsically possess uniaxial negative birefringence, which is due to the average degree of alignment of unit normals to the discs along the director **n** [see Figure 1(b)]. Because of the enormous commercial potential of the liquid crystalline polymer (LCP) products, both rodlike and discotic LCPs attracted more attention since the discovery of the liquid crystalline behavior. After the ultrahigh strength Kevlar fibers made of rodlike LCPs by Dupont were developed in 1971, carbonaceous mesophases which can form the discotic LCPs also found their practical use in the spinning of high performance carbon fibers.[1–3] The performance of LCPs, such as tensile strength and modulus, strongly depend on the orientation configuration of constitutive molecules. In the process of the LCP products, an understanding of the relation between molecular orientation and the flow is useful to obtain the desired performance.

For the last few decades, most of the hydrodynamical theories formulated for flows of LC materials were based on rodlike molecules.[4–10] One of the major advances in the theoretical LCP rheology was made by Doi[8] in 1981, who extended the theory for semidilute polymeric fluids to that for concentrated rodlike polymeric fluids. For the simple shear, the exact solutions of the Doi theory showed that at low shear rates, the orientation distribution function displayed a time-periodic tumbling, followed by the steady-state or flow-aligning, where the director became stationary at high shear rates.[11] And in the region of intermediate shear rates, another different dynamical phenomenon that the director oscillated about a fixed angle was predicted, called "wagging."[12] In general, a phenomenological molecular shape parameter β is introduced into Doi theory, which has been pointed by Ericksen[13] in 1960 that the effect of reducing the aspect ratio can be quite significant, such as from 1.0 to 0.8. This effect due to aspect ratio has been explored in the Refs. 14 and 15 for a variety of

Applied Polymer SCIENCE

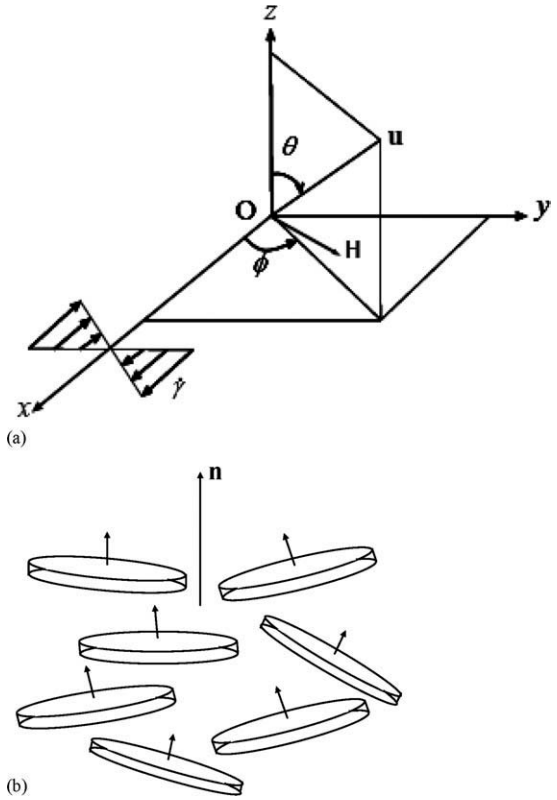

Figure 1. (a) Geometry and co-ordinate systems. (b) Definition of uniaxial director **n** orientation of a discotic nematic LCP. The uniaxial director **n** is the average orientation of the unit normals to the discotic molecules.

mesoscopic closure approximations to the Doi theory. If the infinite aspect ratio nematic liquid is tumbling, lowering aspect ratio will only enhance tumbling. However, a flow-aligned infinite aspect ratio liquid is transformed by lowering aspect ratio to either reduce the Leslie angle downward (toward the flow axis) or cause a tumbling transition. Recently, Singh and Rey[16] used the TR theory[10] to model homogeneous flows of discotic LCPs by reversing the sign of β and showed some promising results. The kinetic theory for spheroidal LCPs developed in Ref. 17 aimed at establishing a unified theory for rodlike and discotic LCPs, which can provide a rigorous justification for the convenient practice and relate the macroscopic parameters to the microscopic ones.

The optimization and control of preferred orientation is practical importance because the mechanical and thermal properties are affected by the degree of alignment and the preferred orientation of discotic molecules. If one can freely control the molecular orientation configuration, the processing optimization may become much simpler. It is well known that the electric or magnetic field imposed on the rodlike LCPs results in the improvement of performance for LCP products.[18,19] Some experiments,[20,21] such as the uses of surface effect and shear flow, were made to obtain alignment phase of discotic LCs. However, the shearing technique requires a special cell and the use of surface effect restricts substrates used. The influence of a magnetic field on the alignment was investigated in the discotic nematic phase of a triphenylene derivative. The uniform alignment was achieved when a magnetic field of 5 T was applied parallel to the cell surface during the cooling process.[22] Also, by application of a magnetic field, Shklyarevskiy et al.[23] found that high mesoscopic order can be introduced in thin films of a hexabenzocoronene-based discotic LC. Forest et al.[24,25] gave a comprehensive study of magnetic field coupled to shear flow for any aspect ratio. The results showed that any limit cycle in any planar flow would be arrested at a critical magnetic field strength for a coplanar magnetic field, which presented the generality and explicated predictions of solving this problem. This generality was also illustrated by a variety of linear flows, such as any kayaking, tumbling, and wagging limit cycle arrested at a critical magnetic field strength. To study the dynamic behaviors of discotic LCPs molecular field, such as the director or stress as a function of time, we will focus our attention on the effect of magnetic fields on the flow-orientation, order parameter, and shear stress of the discotic LCPs in this article. The numerical solution technique is outlined in the Governing equation section. The discussions and conclusions will be presented into the Numerical calculation and Results and discussions sections, respectively.

GOVERNING EQUATION

In this article, we study the microstructural dynamical response of discotic nematic LCPs to a magnetic field. Based on the extended Doi kinetic equation for discotic LCPs discussed by Singh and Rey,[16] the effect of magnetic field on the discotic molecules also is considered, given by

$$\frac{\partial f}{\partial t} = \bar{D}_r \frac{\partial}{\partial \mathbf{u}} \cdot \left(\frac{\partial}{\partial \mathbf{u}} f + f \frac{\partial}{\partial \mathbf{u}} \frac{V(\mathbf{u})}{kT} \right) - \frac{\partial}{\partial \mathbf{u}} \cdot (\dot{\mathbf{u}} f), \tag{1}$$

Here $\bar{D}_r$ denotes the average rotational diffusivity depended on the order parameter tensor **S**:

$$\bar{D}_r = D_s \left(1 - \frac{3}{2} \mathbf{S} : \mathbf{S} \right)^{-2}, \tag{2}$$

where D_s is the rotational diffusivity of an isotropic state. The order parameter tensor **S**, which is the second moment of the orientation distribution f, is defined by the following equation:

$$\mathbf{S} = \int_{|\mathbf{u}|=1} \left(\mathbf{u} - \frac{\mathbf{I}}{3} \right) f dA, \tag{3}$$

here **I** is a unit tensor. When the effect of the magnetic field on the LCP molecules is taken into account, the mean field potential $V(\mathbf{u})$ in eq. (1) can be described as,

$$V(\mathbf{u}) = -\frac{3kTU}{2} \mathbf{S} : \mathbf{uu} - \frac{\mu_0 \Delta\chi}{2} (\mathbf{u} \cdot \mathbf{H})^2, \tag{4}$$

where k (= 1.3806505 × 10^{-23} J/K) is the Boltzmann constant, T the absolute temperature, and U the dimensionless nematic potential intensity. μ_0 (= $4\pi \times 10^{-7}$ H/m) is the

permeability of vacuum, **H** the vector of the magnetic field, and $\Delta\chi$ ($= \chi_{II} - \chi_{\perp}$) the magnetic anisotropy. $\dot{\mathbf{u}}$ in eq. (1) represents the rate of change of **u** by the macroscopic flow, given by

$$\underline{\mathbf{u}} = (\boldsymbol{W} + \beta\boldsymbol{A}) \cdot \mathbf{u} - \mathbf{u} \cdot (\boldsymbol{W} + \beta\boldsymbol{A}) \cdot \mathbf{uu}, \tag{5}$$

here $\boldsymbol{W}$ and $\boldsymbol{A}$ are the corresponding rate-of-strain and vorticity tensors. And the molecular shape parameter, β, is related to the aspect ratio, p, namely,

$$\beta = \frac{p^2 - 1}{p^2 + 1}. \tag{6}$$

β lies among $\beta = -1.0$ for ideal flat discs, $\beta = 0$ for spherical molecules, and $\beta = 1.0$ for infinitely thin rods.

NUMERICAL CALCULATION

Figure 1(a) defines the flow geometry, where x-axis is the flow direction, y-axis is the direction of the velocity gradient, and z-axis is coaxial with the vorticity axis. Figure 1(b) shows the molecular arrangement in typical discotic LCPs, where the shortest molecular dimension aligns along the direction to capture the flow behavior of discotic LCPs.[26] The material is sheared with the shear rate of $\dot{\gamma}$ in the x–y plane, and the rate-of-strain and vorticity tensors are given by,

$$\boldsymbol{A} = \frac{1}{2}\dot{\gamma}\begin{pmatrix} 0 & 1 & 0 \\ 1 & 0 & 0 \\ 0 & 0 & 0 \end{pmatrix}, \quad \boldsymbol{W} = \frac{1}{2}\dot{\gamma}\begin{pmatrix} 0 & 1 & 0 \\ -1 & 0 & 0 \\ 0 & 0 & 0 \end{pmatrix}. \tag{7}$$

The orientation of a single molecule represented by a unit vector **u** is characterized with an azimuthal angle ϕ and a polar angle θ [see Figure 1(a)]. The orientation distribution function f keeps symmetry with respect to the x–y plane, when the director always remains in the shear plane. That is,

$$f(\theta, \phi, t) = f(\pi - \theta, \phi, t), \tag{8}$$

also, it should be mentioned here that as there is no distinction between head and tale of the model rods, the function f must has the point symmetry:

$$f(\theta, \phi, t) = f(\pi - \theta, \pi + \phi, t). \tag{9}$$

From above conditions for the distribution function f, the non-zero components of the order parameter tensor **S** are:

$$\mathbf{S} = \begin{bmatrix} S_{xx} & S_{xy} & 0 \\ S_{xy} & S_{yy} & 0 \\ 0 & 0 & S_{zz} \end{bmatrix}. \tag{10}$$

After nondimensionalization using the time scale $1/Ds$ and the magnetic force $\sqrt{2kT/\mu_0\Delta\chi}$, eq. (1) for one-dimensional magnetic field ($\mathbf{H} = (H_x, H_y, 0)$) becomes

$$\begin{aligned}
\frac{\partial f}{\partial t^*} &= \left(1 - \frac{3}{2}\mathbf{S} : \mathbf{S}\right)^{-2}\left(\frac{\partial^2 f}{\partial\theta^2} + \cot\theta\frac{\partial f}{\partial\theta} + \frac{1}{\sin^2\theta}\frac{\partial^2 f}{\partial\phi^2}\right) \\
&+ 3U\left(1 - \frac{3}{2}\mathbf{S} : \mathbf{S}\right)^{-2}\{3f\left(S_{xx}\sin^2\theta\cos^2\phi + S_{yy}\sin^2\theta\sin^2\phi\right. \\
&+ S_{zz}\cos^2\theta + S_{xy}\sin^2\theta\sin 2\phi) - \frac{1}{2}\frac{\partial f}{\partial\theta}\sin 2\theta\left(S_{xx}\cos^2\phi\right. \\
&+ S_{yy}\sin^2\phi - S_{zz} + S_{xy}\sin 2\phi) \\
&+ \frac{1}{2}\frac{\partial f}{\partial\phi}\left(S_{xx}\sin 2\phi - S_{yy}\sin 2\phi - 2S_{xy}\cos 2\phi\right)\} \\
&+ \left(1 - \frac{3}{2}\mathbf{S} : \mathbf{S}\right)^{-2}\{2f\left[H_x^{*^2}\left(3\sin^2\theta\cos^2\phi - 1\right)\right. \\
&+ H_y^{*^2}\left(3\sin^2\theta\sin^2\phi - 1\right) + 3H_x^*H_y^*\sin 2\phi\sin^2\theta] \\
&- \frac{\partial f}{\partial\theta}\left[\sin 2\theta\left(H_x^{*^2}\cos^2\phi + H_y^{*^2}\sin^2\phi + H_x^*H_y^*\sin 2\phi\right)\right] \\
&+ \frac{\partial f}{\partial\phi}\left[\sin 2\phi\left(H_x^{*^2} - H_y^{*^2}\right) - 2H_x^*H_y^*\cos 2\phi\right]\} \\
&+ \dot{\gamma}^*\left\{\beta\left(\frac{3}{2}f\sin^2\theta\sin 2\phi - \frac{1}{4}\frac{\partial f}{\partial\theta}\sin 2\theta\sin 2\phi\right)\right. \\
&\left. + \frac{\partial f}{\partial\phi}\left(1 - \beta\cos 2\phi\right)/2\right\}
\end{aligned} \tag{11}$$

where

$$\begin{aligned}
\dot{\gamma}^* &= \dot{\gamma}/D_s \\
H_x^* &= H_x/\sqrt{2kT/\mu_0\Delta\chi} \\
H_y^* &= H_y/\sqrt{2kT/\mu_0\Delta\chi} \\
t^* &= tD_s.
\end{aligned} \tag{12}$$

The superscripts * denote nondimensionalized variables and parameters. The above equation is computed using the finite difference method for spatial discretization and the Crank–Nicolson method for time integration. Because of the condition eqs. (8) and (9), the computation area for f can be restricted in the region $0 \le \theta \le \pi/2$ and $-\pi/2 \le \phi \le \pi/2$. Boundary conditions for the function are:

$$\partial f(0, \phi, t^*)/\partial\theta = 0, \tag{13a}$$

$$\partial f(\pi/2, \phi, t^*)/\partial\theta = 0, \tag{13b}$$

$$\partial f(\theta, -\pi/2, t^*) = f(\theta, \pi/2, t^*), \tag{13c}$$

$$\partial f(\theta, -\pi/2, t^*)/\partial\phi = \partial f(\theta, \pi/2, t^*)/\partial\phi. \tag{13d}$$

the normalization condition,

$$4\int_0^{\pi/2} d\theta \int_0^{\pi} d\phi f \sin\theta = 1. \tag{14}$$

is also required. An initial profile of the function, $f(\theta,\phi,t^* = 0)$, is derived from the Boltzmann profile with the major orientation direction along the x-axis (flow direction). The time step and the spatial mesh width are set to be $\Delta t^* = 0.005/\dot{\gamma}^*$ and $\Delta\theta = \Delta\phi = 3°$.

RESULTS AND DISCUSSIONS

Computational parameters in eq. (11) are the dimensionless nematic potential intensity U proportion to concentration of LCPs

Applied Polymer SCIENCE

solutions, the dimensionless magnetic field strengths H_x^* and H_y^*, and dimensionless shear rate $\dot{\gamma}^*$. To make easy to see the effect of the magnetic fields on the order parameter and the shear stress, the nematic potential intensity U is set to be 5, which corresponds to the lowest order of the nematic state after the isotropic-nematic phase transition happens. In the following discussions, the computation results will be mainly organized in terms of the major orientation angle, the scalar order parameter, and the viscosity stress nondimensionalized by $3ckT$, where c denotes the number of discs in unit volume, defined by

$$\tan 2\phi_m = \frac{2S_{xy}}{S_{xx} - S_{yy}}, \tag{15a}$$

$$S = \sqrt{\frac{3}{2}\mathbf{S} : \mathbf{S}}, \tag{15b}$$

and

$$\sigma^*_{\alpha\beta} = S_{\alpha\beta} - U\left(S_{\alpha\mu} < u_\mu u_\beta > - S_{\mu\nu} < u_\mu u_\nu u_\alpha u_\beta >\right), \tag{15c}$$

here $<\ldots>$ stands for the average over the distribution function.

The nondimensionalized first and second normal stress differences are given by

$$N_1^* = \sigma^*_{xx} - \sigma^*_{yy}, \tag{16a}$$

$$N_2^* = \sigma^*_{yy} - \sigma^*_{zz}. \tag{16b}$$

Magnetic Fields Along the *x*-Axis

In this section, we deal with the case that the magnetic field is parallel to the flow direction. Figure 2 shows the time evolutions of the major orientation angle ϕ_m, scalar order parameter S and the first and second normal stress differences N_1^*, N_2^* as a function of strain $\gamma(= t^*\dot{\gamma}^*)$ for $\dot{\gamma}^* = 1.0$ and $H_x^* = 0$, 0.5×10^{-6}, and 0.9×10^{-6}. For $H_x^* = 0$, ϕ_m shows the typical tumbling behavior same with the rodlike nematic LCPs, where ϕ_m periodically decreases with γ. When the magnetic field is imposed, for example $H_x^* = 0.5 \times 10^{-6}$, the decrease period becomes longer. And once a critical magnetic field strength is arrived, $H_x^* = 0.9 \times 10^{-6}$, ϕ_m no longer changes with time and the system shows an aligning like behavior, which is called the new aligning behavior defined in Ref. 18. The behaviors of S reflect the behaviors of ϕ_m, and the steady value of S for $H_x^* = 0.9 \times 10^{-6}$ is slightly higher than that at the equilibrium state. When $H_x^* = 0$, 0.5×10^{-6} N_1^*, N_2^* periodically change with γ in which two peaks can be observed. As described at $H_x^* = 0.9 \times 10^{-6}$, a stable state of N_1^*, N_2^* is achieved caused by the new aligning. Figure 3 shows the time evolutions of ϕ_m, S, and N_1^*, N_2^* as a function of strain $\gamma(= t^*\dot{\gamma}^*)$ for $\dot{\gamma}^* = 3$ and $H_x^* = 0$, 0.9×10^{-6}, and 1.5×10^{-6}. For $H_x^* = 0$, the system exhibits the wagging behavior which oscillates in the $-135° \le \phi_m \le -45°$ sector. As the magnetic field is imposed, for $H_x^* = 0.9 \times 10^{-6}$, the period and the amplitude of the oscillatory behavior of ϕ_m increase. Similar to the case for $\dot{\gamma}^* = 1$, the system shows the new aligning behavior above a certain critical H_x^*. The periodically oscillates of N_1^*, N_2^* will increase when the magnetic field

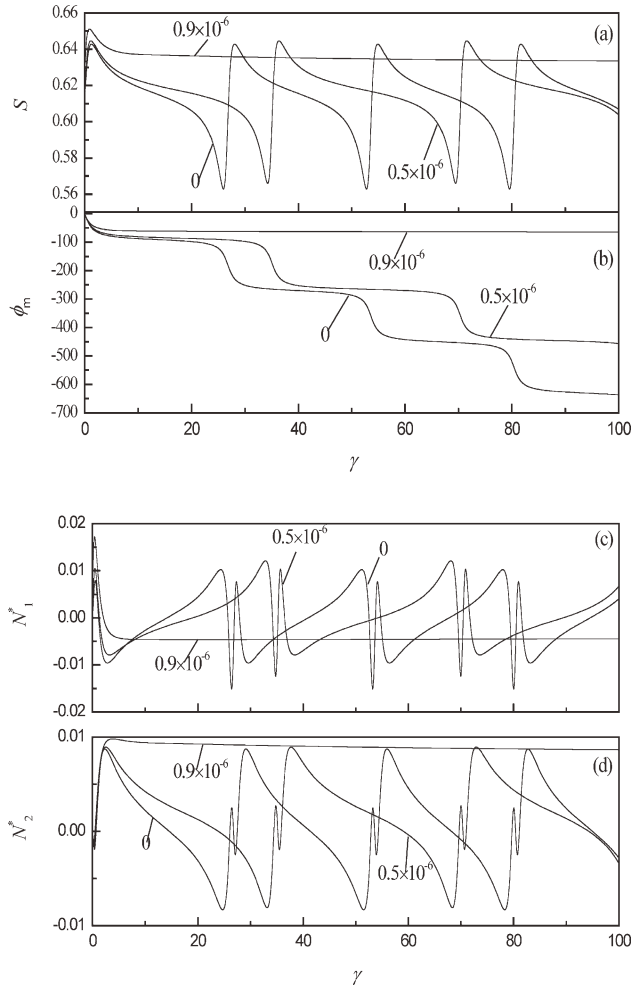

Figure 2. Transient behaviors of ϕ_m, S, and N_1^*, N_2^* versus strain at $\dot{\gamma}^* = 1$ for various values of $H_x^* = 0$, 0.5×10^{-6}, and 0.9×10^{-6} at $\beta = -1.0$.

strength is imposed at 0.9×10^{-6}. Compared with the results for $\dot{\gamma}^* = 1$, stronger magnetic field is necessary for the stable states, such as $H_x^* = 1.5 \times 10^{-6}$. Figure 4 is the time evolution of ϕ_m, S, and N_1^*, N_2^* as a function of strain $\gamma(= t^*\dot{\gamma}^*)$ for $\dot{\gamma}^* = 5$, at which the system without the magnetic field shows the normal aligning behavior. It can be seen that the normal aligning modes can be observed near at $-90°$ and the new aligning mode near at $-60°$, which are the results of the competition of the moments caused by the flow and the magnetic fields. The damping behaviors of N_1^*, N_2^* can be seen at $H_x^* = 0$, 0.9×10^{-6}. However, once the magnetic field strength is beyond the critical value, the steady state results from the new aligning also can be achieved.

The time-averaged first and second normal stress differences ($\bar{N}_1^*$, $\bar{N}_2^*$) are plotted as the function of the shear flow and the magnetic field in Figure 5. When $H_x^* = 0$, the results, where the negative $\bar{N}_1^*$ is observed at lower and higher shear rate regions, are exactly contrary with those conclusions obtained by Larson[12] and Marrucci and Maffettone[11] for the rodlike LCPs. When the magnetic fields are imposed, more complicated changes are presented, where on increasing strength of the

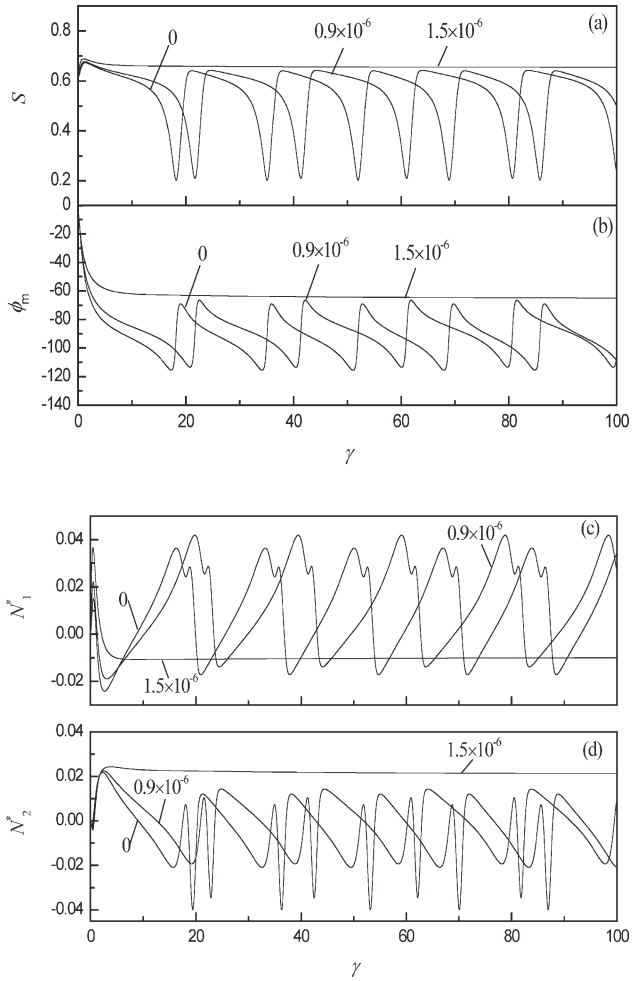

Figure 3. Transient behaviors of ϕ_m, S, and N_1^*, N_2^* versus strain at $\dot{\gamma}^* = 3$ for various values of $H_x^* = 0$, 0.9×10^{-6}, and 1.5×10^{-6} at $\beta = -1.0$.

magnetic fields the negative region of $\bar{N}_1^*$ moves from the lower shear rate to the higher shear rate region and is enlarged further. Same with the rodlike LCPs, the new aligning also is observed which spreads toward the higher shear rate and takes over the whole tumbling and wagging regimes. The mode transition shear rate between the new aligning mode and the normal aligning mode also is identified in the figure when $H_x^* = 2 \times 10^{-6}$. The sign of $\bar{N}_2^*$ becomes positive in all the shear regions, once the effect caused by the shear flow is swamped by the magnetic fields. Compared with Ref. 19 in which the rodlike LCPs is affected by the magnetic fields, $\bar{N}_1^*$, $\bar{N}_2^*$ are almost opposite to the results when the magnetic fields are along the y-axis.

Figure 6 shows the effect of magnetic fields on the time-averaged generalized viscosity $\bar{\eta}^* \left(= \bar{\sigma}_{xy}^*/\dot{\gamma}^*\right)$. To capture the flow characteristic of discotic nematic LCPs, we have to consider the fact that the shortest molecular dimension aligns along the director. Through comparing with the results of rodlike LCPs,[19] the conclusion that the negative viscosity $\bar{\eta}^*$ is a mirror image of that corresponding to rods has been made. In the low shear region, the absolute values of $\bar{\eta}^*$ increase with the magnetic field strength which can be expected if the phase formed by the discotic LCPs under magnetic fields is taken into account. However, all the values of $\bar{\eta}^*$ will be near to zero once the shear rate is large enough.

Magnetic Fields Along the y-Axis

Figure 7 shows that the time-averaged $\bar{N}_1^*$ is plotted as the function of the shear rate and magnetic field strength. It is well known that in this case the magnetic field tends to rotate the director, namely, the shortest axis of the discotic LCPs, into the vorticity direction. In this case, the longest axis is arranged along the shear flow. If the moment caused by the magnetic fields is stronger than that caused by the shear rate, the values of $\bar{N}_1^*$ become negative in all the shear rate regions, such as, $H_y^* = 2 \times 10^{-6}$. The transition of phase among tumbling, wagging, and aligning affected by the magnetic field also is indicated in the figure. Figure 8 plots the ratio $\bar{N}_2^*/\bar{N}_1^*$ as a function of $\dot{\gamma}^*$ with the various magnetic field strength. The absolute ratio $\bar{N}_2^*/\bar{N}_1^*$ increases with the increasing magnetic field strength. From the ratio, $\bar{N}_2^*$ is predicted to be negative in the middle shear rate region.

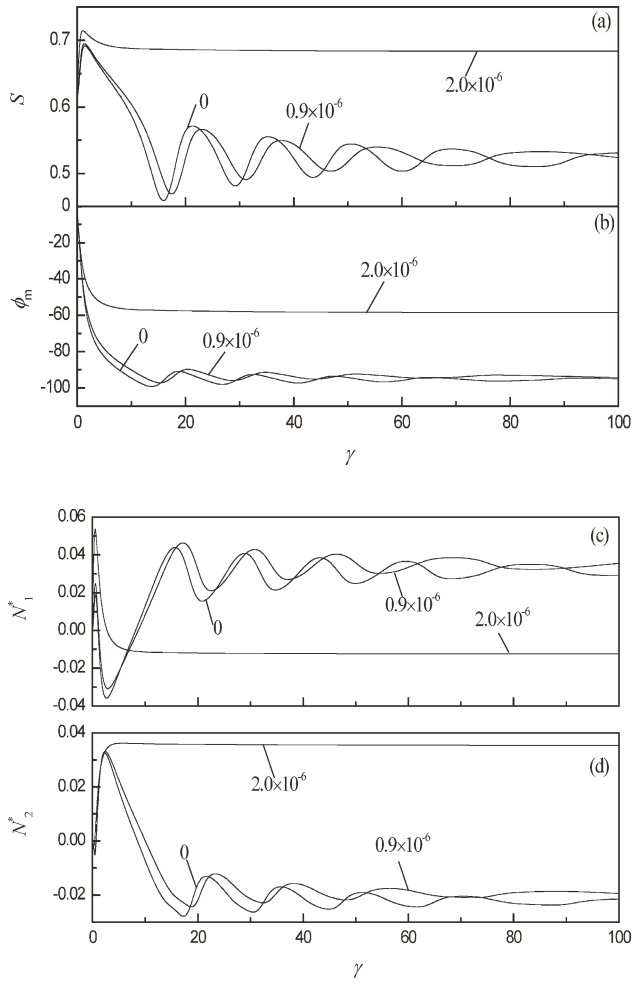

Figure 4. Transient behaviors of ϕ_m, S, and N_1^*, N_2^* versus strain at $\dot{\gamma}^* = 5$ for various values of $H_x^* = 0$, 0.9×10^{-6}, and 2×10^{-6} at $\beta = -1.0$.

Applied Polymer SCIENCE

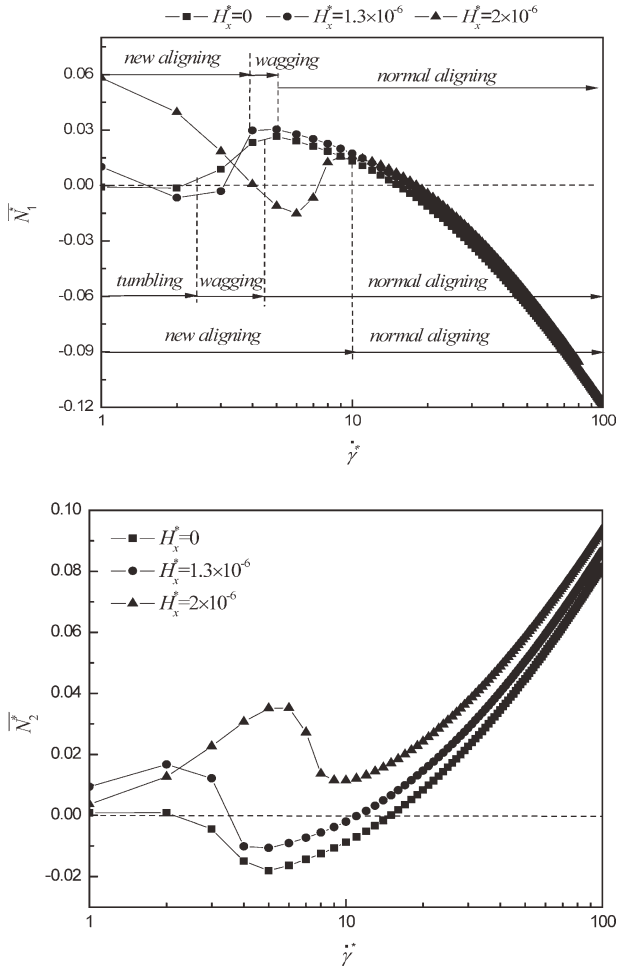

Figure 5. Effect of magnetic field on the time-average first and second normal stress differences $\bar{N}_1^*$ and $\bar{N}_2^*$ with various H_x^* at $\beta = -1.0$.

Flow-Phase Diagram

The effect of the magnetic field on the flow-orientation mode transition is discussed in the Figure 9, where a flow-orientation

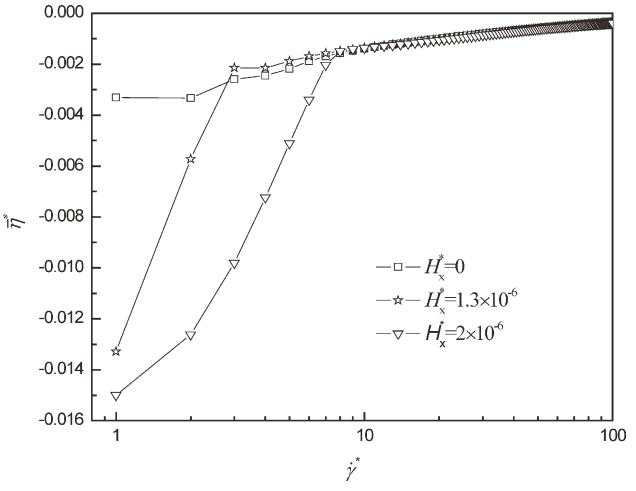

Figure 6. Plot of the time-average generalized viscosity $\bar{\eta}^*$ versus shear rate with various H_x^* at $\beta = -1.0$.

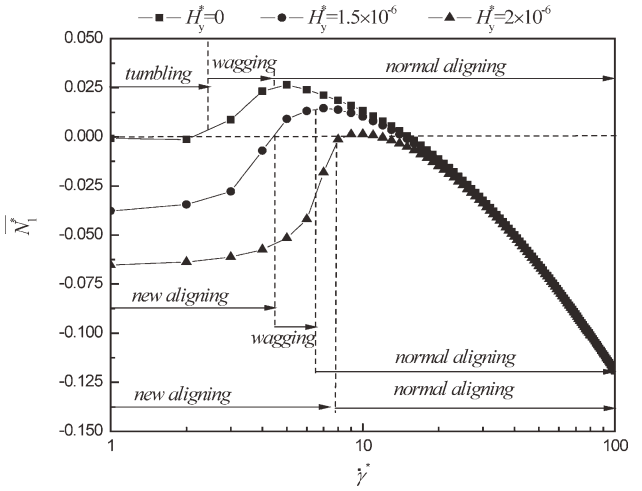

Figure 7. Effect of magnetic fields on $\bar{N}_1^*$ with various H_y^* at $\beta = -1.0$.

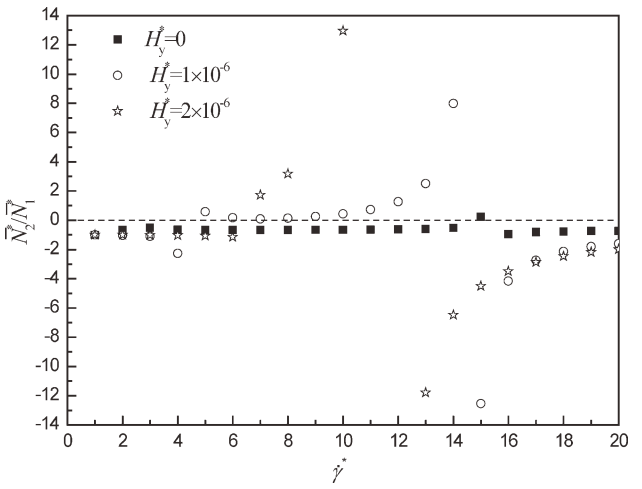

Figure 8. Ratio $\bar{N}_2^*/\bar{N}_1^*$ of the first to the second normal stress differences as a function $\dot{\gamma}^*$ with various H_y^* at $\beta = -1.0$.

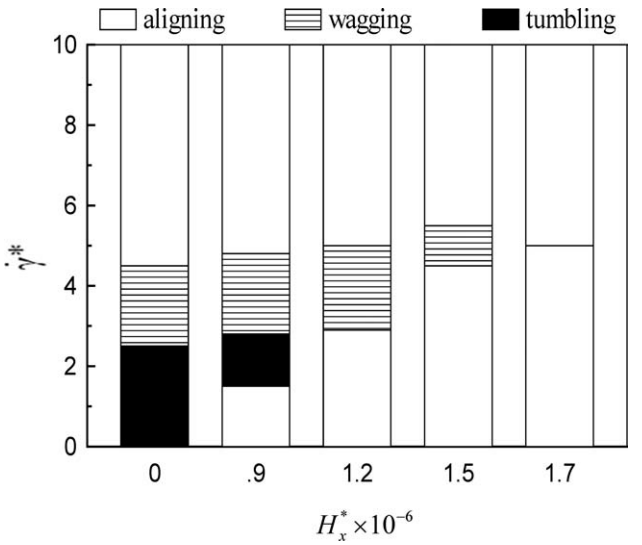

Figure 9. Critical shear rates as a function of magnetic field at $\beta = -1.0$.

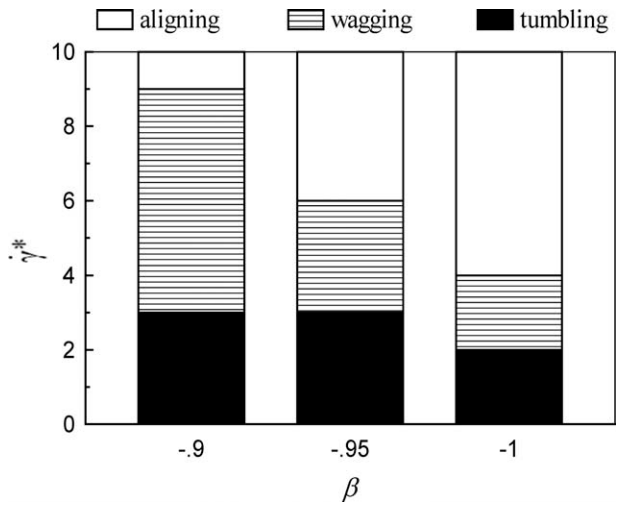

Figure 10. Critical shear rates as a function of β at $H_x^* = 0$.

mode diagram spanned by the shear rate $\dot{\gamma}^*$ and the magnetic field strength H_x^*. For the case that only the shear flow is applied to the system (i.e., $H_x^* = 0$), the tumbling, wagging, and aligning modes appear depending on the shear rate. At $H_x^* = 0.9 \times 10^{-6}$, the new aligning mode regime emerges at low shear rate, erodes the tumbling regime with the increase of H_x^*, and finally the tumbling regime disappears at $H_x^* = 1.2 \times 10^{-6}$. The wagging mode regime also disappears, when H_x^* is increased up to 1.7×10^{-6}. A line at $H_x^* = 1.7 \times 10^{-6}$ represents the mode transition shear rate between the new aligning mode and the normal aligning mode. It is expected that the transition shear rate becomes higher if H_x^* is increased furthermore. To show the effect of β on the phase diagram, the flow-orientation mode transition versus β is investigated in Figure 10, when the magnetic field strength is zero. It is found that the regions of tumbling and wagging will be enlarged with the increasing β, for example, $\beta = -0.9$. It is expected that similar results will be achieved when the magnetic field is applied to the y-axis.

CONCLUSIONS

In this article, the dynamic behavior of discotic nematic LCPs is investigated when the magnetic field is applied on the flow. The extended Doi equation for discotic LCPs is calculated without using any closure approximation. When only the shear rate is imposed, the similarity with the various regimes of rodlike LCPs in the shear flow, which is in good agreement with the conclusions presented by Farhoudi and Rey,[27] is obtained. Due to the moment caused by the magnetic field stronger than that caused by the shear flow the new aligning state defined in the Ref. 18 also is found at low shear rate region. The sign changes of the time-averaged $\bar{N}_1^*$ and $\bar{N}_2^*$ are completely opposite with those results obtained for rodlike LCPs by the Refs. 18 and 19. In addition, as the mirror images of rodlike LCPs the values of $\bar{\eta}^*$ are negative in the entire shear rate regions. It may be responsible by the shortest major axis of discotic LCPs molecules arranged along the director. Finally, we also predict the phase diagram among tumbling, wagging, aligning, and new aligning versus the magnetic fields at $\beta = -1.0$. The effect of molecular shape on the phase transition also is discussed as the results obtained by the simulation are suited to the infinite discotic nematic LCPs. Besides, if we consider that at the room temperature, the magnetic field strength of 1.0×10^{-6} is imposed on HBC-PhC$_{12}$, a discotic liquid-crystalline semiconductor with $\Delta\chi = 4.9 \times 10^{-9}$ m^3/mol, the real magnetic field strength will be about 0.643 T which can be got in the laboratory.

To illustrate the effect of the moments on the final state of the discotic LCPs, Figure 11 presents the moments and deformation caused by the shear flow and the magnetic field along the x- and y-axis, respectively. From the previous results of Farhoudi and Rey[27] and Takserman-Krozer and Ziabicki,[28] it follows that when the director of a discotic LCPs is oriented along an extension direction, the degree of S decreases, but it increases when orientated along a compression director [shown in Figure 11(a)]. As it can be seen from Figure 11(b,c), the moments caused by the magnetic fields always rotate the director along their direction. The deformation caused by the moments also is shown in the figure. The result of competition between the moments caused by the shear flow and the magnetic fields will decide the final state of discotic LCPs.

Through this computation many interesting results, which are almost reversed to those obtained from rodlike LCPs, such as, the shear stress and the generalized viscosity, are presented. If we can control the strength and direction of the magnetic fields freely, the expected performance of discotic LCPs will be achieved.

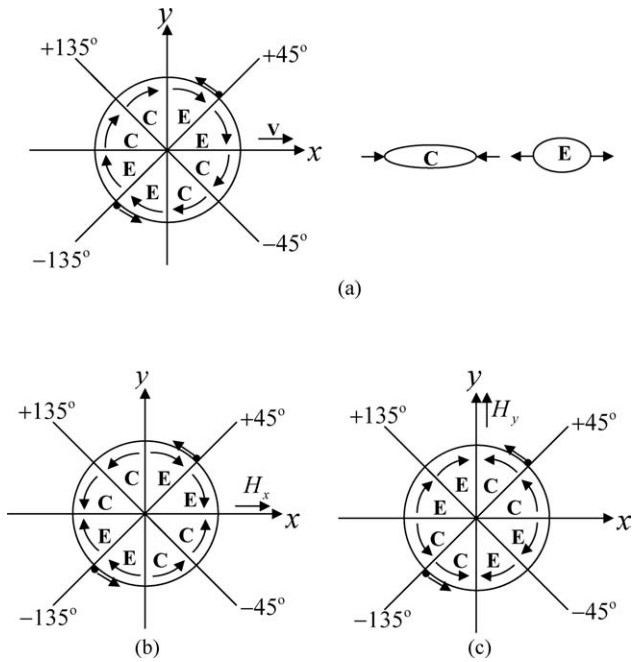

Figure 11. (a) Torque map and deformation for a discotic phase, which is affected only by the shear flow along the x-axis. (b) and (c) Torque map and deformation caused the magnetic fields imposed along the x- and y-axis, respectively.

ACKNOWLEDGMENTS

This work is supported by the National Natural Science Foundation of China through grant 11104050 and Young Academic Backbone of Education Commission Heilong Jiang Province through grant 1251G030. The authors also thank Drs. Tomohiro Tsuji and Shigeomi Chono for useful discussions.

REFERENCES

1. Otani, S. *Mol. Cryst. Liq. Cryst.* **1981,** *63*, 249.
2. Zimmer, J. E.; White, J. L. In Advances in Liquid Crystals, Vol. *5*; Brown, H. G., Ed.; Academic Press: New York, **1982.**
3. Singer, L. S. *Faraday Discuss. Chem. Soc.* **1985,** *73*, 265.
4. Hess, S. *Z. Naturforsch* **1976,** *A31a*, 1034.
5. Leslie, F. M. *Adv. Liq. Cryst.* **1979,** *4*, 1.
6. Hand, G. L. *J. Fluid Mech.* **1962,** *13*, 33.
7. Beris, A. N.; Edwards, B. J. Thermodynamics of Flowing Systems with Internal Microstructure; Oxford Science Publications: New York, **1994.**
8. Doi, M. *J. Polym. Sci. Polym. Phys. Ed.* **1981,** *19*, 229.
9. Marrucci, G.; Greco, F. *Mol. Cryst. Liq. Cryst.* **1991,** *206*, 17.
10. Tsuji, T.; Rey, A. D. *J. Non-Newtonian Fluid Mech.* **1997,** *73*, 127.
11. Marrucci, G.; Maffettone, P. L. *Macromolecules* **1989,** *22*, 4076.
12. Larson, R. G. *Macromolecules* **1990,** *23*, 3983.
13. Ericksen, J. L. *Arch. Ration. Mech. Anal.* **1960,** *4*, 231.
14. Forest, M. G.; Wang, Q. *Rheol. Acta* **2003,** *42*, 20.
15. Forest, M. G.; Zhou, R.; Wang, Q. *J. Non-Newtonian Fluid Mech.* **2004,** *116*, 183.
16. Singh, A. P.; Rey, A. D. *J. Rheol. Acta* **1998,** *37*, 30.
17. Wang, Q. *J. Chem. Phys.* **2002,** *116*, 9120.
18. Fu, S.; Tsuji, T.; Chono, S. *J. Rheol.* **2008,** *52*, 451.
19. Fu, S.; Wang, X.-Z. *J. Polym. Sci. Part B: Polym. Phys.* **2010,** *48*, 1919.
20. Perova, T. S.; Vij, J. K. *Adv. Mater.* **1995,** *7*, 919.
21. Mang, J. T.; Kumar, S.; Hammouda, B. *Europhys. Lett.* **1994,** *28*, 489.
22. Ikeda, S.; Takanishi, Y.; Ishikawa, K.; Takezoe, H. *Mol. Cryst. Liq. Cryst.* **1999,** *329*, 589.
23. Shklyarevskiy, I. O.; Jonkheijm, P.; Stutzmann, N.; Wasserberg, D.; Wondergem, H. J.; Christianen, P. C. M.; Schenning, A. P. H. J.; de Leeuw, D. M.; Tomovic, Z.; Wu, J.; Mullen, K.; Maan, J. C. *J. Am. Chem. Soc.* **2005,** *127*, 16233.
24. Forest, M. G.; Sircar, S.; Wang, Q.; Zhou, R. *Phys. Fluids* **2006,** *18*, 103102.
25. Forest, M. G.; Wang, Q.; Zhou, R. *J. Rheol.* **2007,** *51*, 1.
26. deGennes, P. G. The Physics of Liquid Crystals; Oxford University Press: London, **1975;** pp 153–165.
27. Farhoudi, Y.; Rey, A. D. *J. Rheol. Acta* **1993,** *32*, 207.
28. Takserman-Krozer, R.; Ziabicki, A. *J. Polym. Sci. Part A: Gen. Pap.* **1963,** *1*, 491.